Scientia Iranica A (2019) 26(2), 634–649

Sharif University of Technology
Scientia Iranica
Transactions A: Civil Engineering
http://scientiairanica.sharif.edu

Analysis of RC beams strengthened with FRP sheets under shear and flexure using MCFT

D. Mostofinejad[a] and M. Noormohamadi[b,*]

a. *Department of Civil Engineering, Isfahan University of Technology (IUT), Isfahan, Iran.*
b. *Department of Civil Engineering, Sama Technical and Vocatinal Training College, Islamic Azad University, Saveh Branch, Saveh, Iran.*

Received 6 September 2016; received in revised form 10 June 2017; accepted 7 January 2019

KEYWORDS
Debonding;
FRP sheets;
Modified Compression Field Theory (MCFT);
Reinforced concrete;
Shear strengthening.

Abstract. Shear behavior of Reinforced Concrete (RC) beams strengthened with Fiber Reinforced Polymer (FRP) sheets is studied in this paper using Modified Compression Field Theory (MCFT). The beam was considered to be under the combined effects of shear force and bending moment. Equilibrium and compatibility equations as well as stress-strain relationships were developed for an element in the strengthened beam. Due to the extensive computations, a computer program was developed to solve the governing equations. The accuracy of the presented method was verified by the experimental results of 84 strengthened RC beams reported in the literature. Comparison between the measured and predicted results showed that the method could predict the shear behavior of the beam in its entire range up to failure. The method could also incorporate the effect of debonding of the FRP sheets in the analysis. The results of a case study indicated that preventing the debonding of FRP sheets in the web of the beam would significantly increase the shear capacity and, in certain cases, change the failure mode from brittle to ductile.

1. Introduction

Strengthening of RC members with FRP sheets has attracted the attention of many researchers and engineers in the past two decades. More attention has been drawn by flexural strengthening of RC beams than by shear strengthening. Among the available research on the behavior of RC beams strengthened with FRP sheet for shear, very few analytical studies can be found on the behavior of such beams throughout the loading process from zero to failure. Most of the research in this field has been focused on the ultimate shear capacity of the beam and debonding strain of FRP rather than a comprehensive load-deformation history [1-18]. Among the few studies that have investigated the entire behavior of RC beams under shear from the beginning of loading to failure is the one by Malek and Saadatmanesh [19]. Gendron et al. (1999) also studied the shear behavior of RC beams strengthened with FRP sheets [20]. It is noteworthy that debonding of FRP sheets was included in neither of the aforementioned studies.

Shear transfer in RC beams is carried out by several mechanisms including (a) shear resistance developed by the uncracked concrete in the compression zone; (b) interfacial shear transfer by aggregate interlocking in the cracked concrete; and (c) dowel action of the longitudinal reinforcement. Due to the complexity of shear transfer mechanism in RC members, it is difficult to determine the actual stresses in different portions of the beam; therefore, taking advantage of the lower-bound plasticity theory can be a unique

*. *Corresponding author.*
E-mail addresses: dmostofi@cc.iut.ac.ir (D. Mostofinejad); mohsen.noo@Gmail.com (M. Noormohamadi)

doi: 10.24200/sci.2019.21228

procedure for overcoming such deficiency. Based on this theory, truss analogy model and compression force path method are used to determine the internal stresses and the ultimate shear capacity of the beam. In this technique, each stress distribution that satisfies equilibrium conditions can be assumed as internal stress distribution without the need to satisfy deformation compatibility. Based on the lower-bound plasticity theory, the computed shear capacity using the assumed stresses is in the safe margin if the redistribution of stresses is possible (ductile behavior) [21]. Therefore, the truss analogy model and the compression force path method that only satisfy the equilibrium conditions (without satisfying the deformation compatibility) are only suitable for ductile members like under-reinforced RC beams. However, in the case of strengthening of concrete members with a brittle material like FRP composites, the analysis of stresses cannot be performed using the lower-bound plasticity theory. It is mostly because FRP materials, despite their high strain capacities, are non-ductile; thus, they cannot accommodate any stress redistribution. Similarly, concrete is brittle; therefore, stress redistribution cannot be developed in concrete members strengthened with FRP sheets for shear enhancement [21].

Modified Compression Field Theory (MCFT) is capable of determining the actual stresses in different portions of an RC beam by satisfying the equilibrium and compatibility equations using stress-strain relationships of concrete and steel. Therefore, the use of this theory in the analysis of concrete beams is not contingent upon the general conditions of the lower-bound plasticity theory, e.g., the ductile behavior of the members; therefore, it is applicable in the stress analysis of the RC beams strengthened with FRP sheets for shear. In the MCFT, despite the compression field theory and the truss analogy model, tensile strength of concrete is not neglected and there are no simplifying assumption leading to the approximation of the results [22]. In the present study, the MCFT is used to investigate the behavior of strengthened RC beams under shear and flexure. In this method, despite the procedures presented by other researchers, the stress and strain variation through the beam height is calculated and the tensile strength of the concrete is not neglected. Any arbitrary section can be modeled in this method and the FRP sheet can be modeled in any two directions, if needed. Furthermore, this method is able to predict the failure mode of the beam, including debonding of FRP sheets. In fact, there is not any simplifying assumption in the method which causes noticeable approximation in the results. To perform the analysis, the conventional equilibrium and compatibility equations in the MCFT are modified and expanded for concrete members strengthened with FRP sheets.

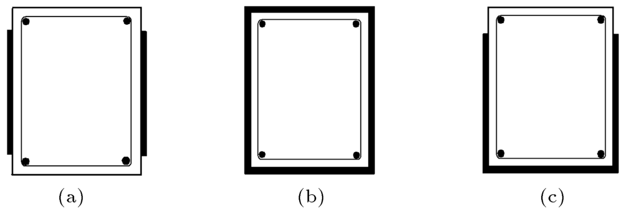

Figure 1. Shear strengthening patterns.

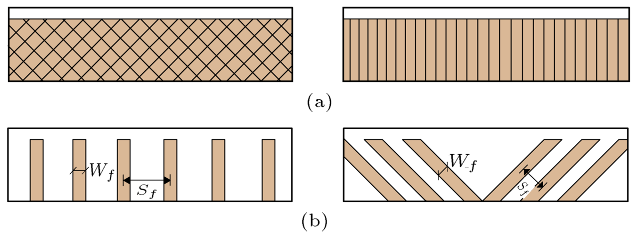

Figure 2. Different configurations for shear strengthening with FRP sheet: (a) Continuously with FRP sheets, and (b) intermittently with FRP strips.

The more popular methods of strengthening RC beams for shear using FRP are as follows:

1. *Side bonding of FRP sheets (Figure 1(a)).* Most of the beams strengthened in this pattern fail due to debonding of FRP sheets [2];
2. *Full wrapping of FRP around beam section (Figure 1(b)).* In most of the beams strengthened in this pattern, due to concrete confinement provided by full wrapping, failure starts with diagonal crushing of the concrete in the web and ends with fracture of FRP sheets [2];
3. *U-shape pattern of FRP composites (Figure 1(c)).* Beams strengthened through this method have unpredictable behavior, i.e., they may fail due to either debonding or fracture of FRP materials.

Note that each of the above strengthening patterns can be used either continuously along the shear span or intermittently with certain width and pitch. Furthermore, FRP fibers can be used in one or two directions. Figure 2 shows some of the possible applications of the FRP sheet along the beam for shear strengthening.

2. Expanding MCFT for members strengthened with FRP sheets

In the modified compression field theory, the behavior of a membrane RC element with a grid of longitudinal and transverse reinforcing bars is investigated. In this section, the theoretical relationships of the method are expanded for an RC element strengthened with FRP. For this purpose, it is assumed that the membrane element of concrete is strengthened with a layer of FRP in addition to the reinforcing longitudinal and

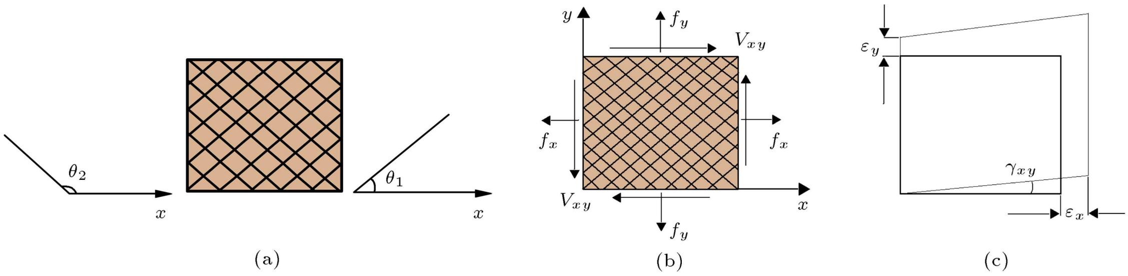

Figure 3. (a) Reinforced concrete element strengthened with FRP sheets. (b) Applied stresses to the element. (c) Deformations due to applied stresses.

transverse steel bars. Orientation of the fibers of the FRP sheets is assumed to be in two arbitrary angles of θ_1 and θ_2, as shown in Figure 3(a).

The in-plane external stresses on the element and the deformations due to the applied stresses are shown in Figure 3(b) and (c), respectively. In these figures, f_x and f_y are the applied normal stresses to the RC element in the x and y directions, respectively, ε_x and ε_y are the strains of RC element in the x and y directions, respectively, v_{xy} is the applied shear stress to the RC element, and γ_{xy} is the shear strain of the RC element. The stresses and strains in the load-carrying components of this element are determined by expanding the compatibility and equilibrium equations and the stress-strain relationships for the strengthened concrete element with an FRP layer.

2.1. Compatibility conditions

Assuming that there is no slip between the concrete and the reinforcing bars as well as between the concrete and FRP sheets, the concrete exhibits compatible deformations with the longitudinal and transverse reinforcing bars and the FRP sheets at the interface. This compatibility is expressed in Eqs. (1) and (2), in which ε_x and ε_y are the strains of RC element in the two perpendicular directions (x and y), ε_{cx} and ε_{cy} are the strains of the concrete in the x and y directions, ε_{sx} and ε_{sy} are the strains of longitudinal and transverse steel bars in the x and y directions, and ε_{fx} and ε_{fy} are the strains of fibers of the FRP in the x and y directions, respectively:

$$\varepsilon_{sx} = \varepsilon_{fx} = \varepsilon_{cx} = \varepsilon_x, \tag{1}$$

$$\varepsilon_{sy} = \varepsilon_{fy} = \varepsilon_{cy} = \varepsilon_y. \tag{2}$$

Other compatibility expressions in the element presented in Eqs. (3), (4), and (5) are derived from the Mohr's circle of strains, as indicated in Figure 4, in which ε_1 and ε_2 are the principal strains in concrete element and θ is the angle of plane of principal strain.

$$\gamma_{xy} = 2(\varepsilon_1 - \varepsilon_x)\tan\theta, \tag{3}$$

$$\varepsilon_x + \varepsilon_y = \varepsilon_1 + \varepsilon_2, \tag{4}$$

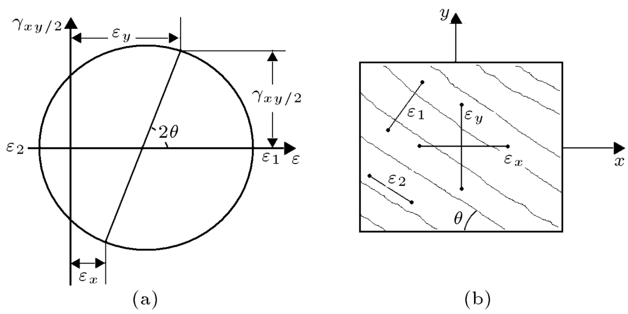

Figure 4. (a) Mohr's circle of strain. (b) Mean strains in RC element.

$$\tan^2\theta = \frac{\varepsilon_x - \varepsilon_2}{\varepsilon_y - \varepsilon_2} = \frac{\varepsilon_1 - \varepsilon_y}{\varepsilon_1 - \varepsilon_x} = \frac{\varepsilon_1 - \varepsilon_y}{\varepsilon_y - \varepsilon_2} = \frac{\varepsilon_x - \varepsilon_2}{\varepsilon_1 - \varepsilon_x}. \tag{5}$$

To determine the stresses in FRP in θ_1 and θ_2 directions, the strains in these directions are needed. If the three components of strain, namely ε_x, ε_y, and γ_{xy}, are determined, the strain values in any arbitrary direction can be calculated using the Mohr's circle of strains or the strain transformation relationships. Thus, having ε_x, ε_y, and γ_{xy}, the strain transformation relationships can be used to determine the strain in the FRP in θ_1 and θ_2 directions. The strain tensor in LT coordinate system with rotation of α can be calculated in accordance with Eq. (6), in which the matrices ε, ε', and r are the strain tensors in the xy and LT coordinate systems and the rotation transformation matrix, respectively:

$$[\varepsilon'] = [r][\varepsilon][r]^T \Rightarrow \begin{bmatrix} \varepsilon_L & \frac{1}{2}\gamma_{LT} \\ \frac{1}{2}\gamma_{LT} & \varepsilon_T \end{bmatrix} = \begin{bmatrix} \cos\alpha & \sin\alpha \\ -\sin\alpha & \cos\alpha \end{bmatrix} \times \begin{bmatrix} \varepsilon_x & \frac{1}{2}\gamma_{xy} \\ \frac{1}{2}\gamma_{xy} & \varepsilon_y \end{bmatrix} \times \begin{bmatrix} \cos\alpha & -\sin\alpha \\ \sin\alpha & \cos\alpha \end{bmatrix}. \tag{6}$$

Performing the above matrix multiplication, the strain values in the LT coordinate system are expressed as follows:

$$\begin{bmatrix} \varepsilon_L \\ \varepsilon_T \\ \gamma_{LT} \end{bmatrix}$$

$$= \begin{bmatrix} \cos^2\alpha & \sin^2\alpha & \sin\alpha\cos\alpha \\ \sin^2\alpha & \cos^2\alpha & -\sin\alpha\cos\alpha \\ -2\sin\alpha\cos\alpha & 2\sin\alpha\cos\alpha & \cos^2\alpha - \sin^2\alpha \end{bmatrix}$$

$$\times \begin{bmatrix} \varepsilon_x \\ \varepsilon_y \\ \gamma_{xy} \end{bmatrix}$$

Thus, if the direction of fibers in the FRP sheets is along the L axis, the strains in the FRP in the θ_1 and θ_2 directions can be calculated by Eqs. (7) and (8), respectively:

$$\varepsilon_{f1} = \varepsilon_x \cos^2\theta_1 + \varepsilon_y \sin^2\theta_1 + \gamma_{xy} \sin\theta_1 \cos\theta_1, \tag{7}$$

$$\varepsilon_{f2} = \varepsilon_x \cos^2\theta_2 + \varepsilon_y \sin^2\theta_2 + \gamma_{xy} \sin\theta_2 \cos\theta_2. \tag{8}$$

2.2. Equilibrium conditions

Figure 5 illustrates the free body diagram of an RC element strengthened with FRP sheets. The stresses in the concrete, reinforcing bars, and FRP sheets due to the applied stresses of f_x, f_y, and v_{xy} are shown in the figure, where v_{cxy} is the shear stress in concrete, and f_{f1} and f_{f2} are the stresses in fibers in θ_1 and θ_2 directions, respectively. Equilibrium in this free body diagram leads to Eq. (9):

$$f_x A = f_{cx} A_c + f_{sx} A_{sx} + f_{f1} \cdot 2d \cdot t_{f1} \cos^2\theta_1 + f_{f2} \cdot 2d \cdot t_{f2} \cos^2\theta_2, \tag{9}$$

where A_c is the net section area of concrete in the RC element and d is the element dimension. Neglecting the decrease in the concrete section area by the section area of the longitudinal reinforcing bars and assuming $A = A_c$ (A is cross section area of the RC element), Eq. (9) can be manipulated in the form of Eq. (10):

$$f_x = f_{cx} + \rho_{sx} f_{sx} + \rho_{f1} f_{f1} \cos^2\theta_1 + \rho_{f2} f_{f2} \cos^2\theta_2, \tag{10}$$

where ρ_{sx} is the ratio of the longitudinal reinforcing bars, and ρ_{f1} and ρ_{f2} are ratios of the fibers in θ_1 and θ_2 directions, respectively, i.e., $\rho_{sx} = A_{sx}/A$, $\rho_{f1} = 2t_{f1}/b$, and $\rho_{f2} = 2t_{f2}/b$, where A_{sx} is the section area of longitudinal reinforcing bars in the RC elements, b is the thickness of the element, and t_{f1} is the thickness of FRP in θ_1 direction.

Similarly, satisfying the equilibrium in y direction for a section perpendicular to section 1-1 (Figure 5) in the element leads to Eq. (11):

$$f_y = f_{cy} + \rho_{sy} f_{sy} + \rho_{f1} f_{f1} \sin^2\theta_1 + \rho_{f2} f_{f2} \sin^2\theta_2, \tag{11}$$

where $\rho_{sy} = A_{sy}/A$ is the ratio of the transverse reinforcing bars and A_{sy} is the section area of transverse reinforcing bars in the element. Neglecting the shear resistance of longitudinal and transverse reinforcing bars and FRP sheets, the shear stress in the concrete equals the applied shear stress to the element, i.e., $v_{cxy} = v_{xy}$.

On the other hand, using the Mohr's circle of stresses (Figure 6(a)) or the equilibrium equations in a concrete element under the stresses of f_{cx}, f_{cy}, and v_{cxy} (Figure 6(b)), the equilibrium equations are obtained in the form of Eqs. (12), (13), and (14):

$$f_{cx} = f_{c1} - v_{cxy}/\tan\theta_c, \tag{12}$$

$$f_{cy} = f_{c1} - v_{cxy}\tan\theta_c, \tag{13}$$

$$f_{c2} = f_{c1} - v_{cxy}(\tan\theta_c + 1/\tan\theta_c), \tag{14}$$

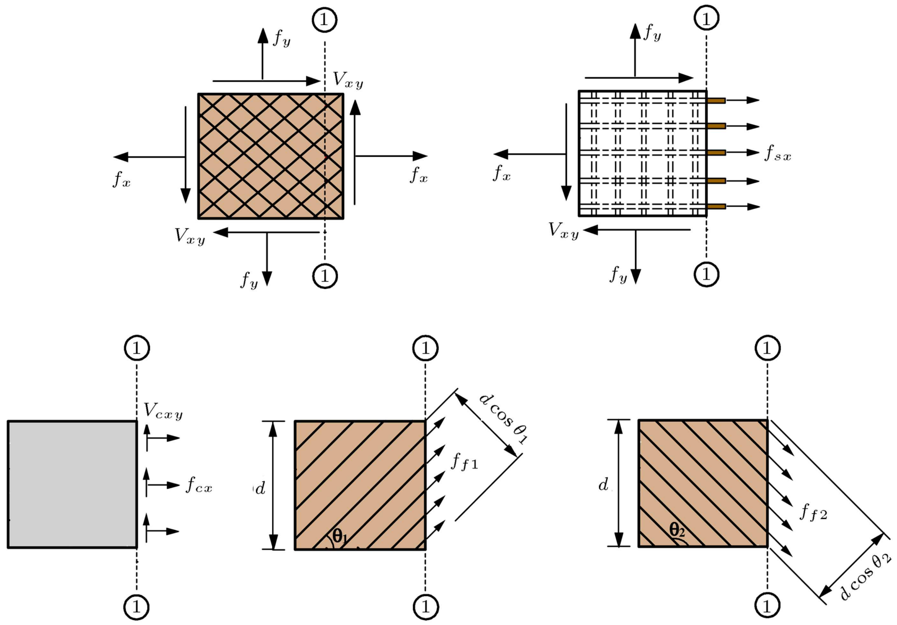

Figure 5. A typical strengthened element and associated free body diagram in section 1-1.

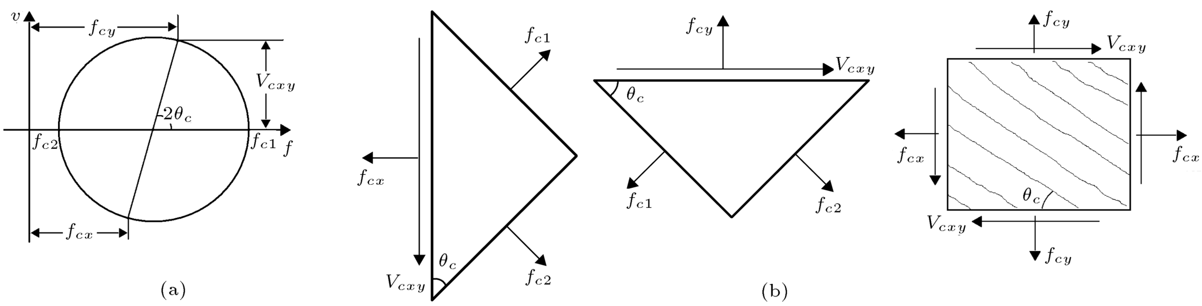

Figure 6. (a) Mohr's circle of strain in concrete. (b) Stresses in concrete.

where θ_c is the inclination angle of the principal plane of stress toward x axis, and f_{c1} and f_{c2} are the tensile and the compressive principal stresses in the concrete, respectively.

For the sake of simplicity, the principal planes of stress and strain in concrete are taken identical ($\theta = \theta_c$). This assumption has experimentally been verified by Vecchio and Collins [22].

2.3. Stress-strain relationship

Based on the compatibility of deformations and equilibrium of forces in an RC element strengthened with FRP sheets, the stress-strain relationships of steel, concrete, and FRP are used to relate the stress and strain components in the element. Bilinear stress-strain relationship in longitudinal and transverse reinforcing bars is used, i.e., $f_s = E_s\varepsilon_s \leq f_y$, where E_s is the modulus of elasticity of steel, and ε_s and f_y are the strain and yield strengths of the longitudinal or transverse reinforcing bars, respectively.

To complete the model, the relationships between the principal compressive and tensile stresses and the principal compressive strains in the concrete are needed. In the RC element under discussion, the compressive strength of concrete is much less than the compressive strength of concrete cylinder, particularly due to considerable amount of tensile strain perpendicular to the compressive strain. For this reason, Eqs. (15) and (16) are used as the stress-strain relationships of concrete [22]:

$$f_{c2} = f_{c2\,\max}\left(2(\frac{\varepsilon_2}{\varepsilon'_c}) - (\frac{\varepsilon_2}{\varepsilon'_c})^2\right), \tag{15}$$

$$f_{c2\,\max} = \frac{f'_c}{0.8 - 0.34\varepsilon_1/\varepsilon'_c} \leq f'_c, \tag{16}$$

where $f_{c2\,\max}$ is the compressive strength of concrete when the tensile stresses are present in the perpendicular direction, f'_c is the compressive strength of the concrete cylinder, and ε'_c is the strain of concrete corresponding to its compressive strength.

Eqs. (15) and (16) show that due to the presence of tensile strains in the perpendicular direction to the compressive strains, the compressive strength of the element under investigation is less than the uniaxial compressive strength of the concrete cylinder, and the $f_{c2\,\max}/f'_c$ ratio decreases with an increase in ε_1.

Tensile strength of concrete is included in the current study to increase the accuracy of the results. It is neglected in many available models and methods, including the compression field theory and the truss analogy models. Therefore, the results of such methods are considerably conservative. In the present study, the relationship between the principal tensile stress and strain in concrete is expressed by Eq. (17), which is adopted from Vecchio and Collins [22]:

$$f_{c1} = \begin{cases} E_c\varepsilon_1 & \text{if } \varepsilon_1 \leq \varepsilon_{cr} \\ \frac{f_{cr}}{1+\sqrt{200\varepsilon_1}} & \text{if } \varepsilon_1 > \varepsilon_{cr} \end{cases} \tag{17}$$

where f_{cr} and ε_{cr} are the stress and strain corresponding to cracking of concrete in tension. Eq. (17) expresses a linear stress-strain relationship up to cracking of concrete in tension and a non-linear descending branch for stress-strain relationship of concrete after cracking.

A linear behavior up to failure is assumed for FRP sheets as it is stipulated in ACI 440 [23], i.e., $f_f = E_f\varepsilon_f$, in which E_f is the modulus of elasticity of FRP, and f_f and ε_f are the stress and the strain in the FRP, respectively.

3. RC beams strengthened with FRP sheets

After the expansion of equilibrium and compatibility equations and the stress-strain relationships to an RC membrane element strengthened with FRP sheets, the behavior of a strengthened RC beam with FRP sheets is investigated. To solve the equations and analyze the beam, a layer model approach is used [24] in which the beam section is divided horizontally into concrete and steel layers and each concrete layer contains the FRP bonded to the beam section sides (Figure 7).

To analyze the beam, an assumed strain diagram is selected (Figure 7); then, the equilibrium and the compatibility conditions in each layer (as a membrane element) are satisfied. Finally, the overall equilibrium of the shear force, axial force, and bending moment

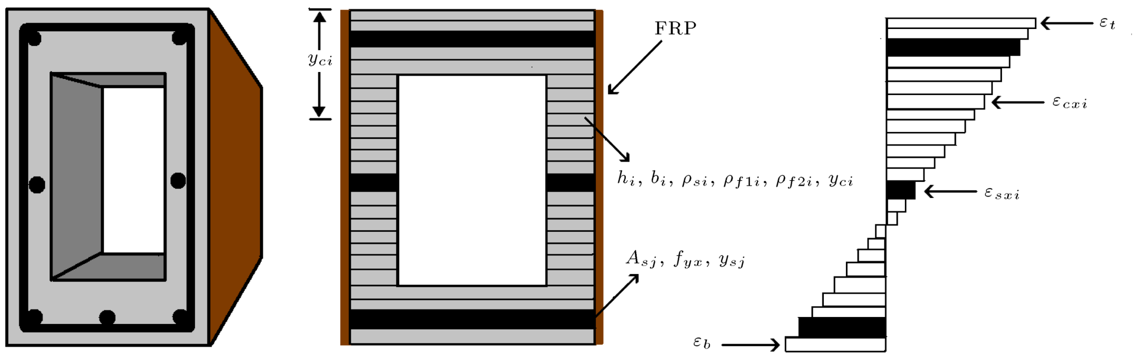

Figure 7. layer model and longitudinal strain distribution in an RC beam strengthened with FRP sheets.

is checked. The analysis is performed under certain forces applied to the beam, i.e., under certain shear and axial forces and flexure; then, the stress and strain components at all layers are determined.

Calculation of the FRP reinforcement ratio in the section of strengthened beam depends on the condition of continuity of the FRP sheets along the beam length. If continuous FRP sheets are used for shear strengthening (Figure 2(a)), the FRP reinforcement ratio, ρ_f, is computed as $\rho_f = 2t_f/b_w$, where b_w is the web width and t_f is the thickness of FRP sheets. On the other hand, for RC beams strengthened for shear with intermittent FRP sheets (Figure 2(b)), the FRP ratio is computed as $\rho_f = 2t_f w_s/b_w s_f$, where w_f and s_f are the width of the FRP sheets and spacing of the sheets, respectively; both of them are determined as shown in Figure 2(b) for the vertical or inclined sheets.

A computer program named Shear Analysis 2 (SA2) was developed to perform the analysis. The program performed high volume of calculations based on trial and adjustment procedures to analyze a particular strengthened RC beam.

The ultimate failure of FRP and its probable debonding from the concrete surface have to be included and checked in the analysis. Since in SA2 program, the information on the stresses and strains is available for all load-carrying elements of the beam (concrete layers, steel, and FRP), it is simply feasible to limit the strains in FRP composites in each layer to predefined strains corresponding to failure or debonding of the FRP sheets. Many relations have been presented in the literature to determine the limiting strain corresponding to debonding of FRP sheets, e.g., the equations suggested by Chen and Teng [25], Khalifa et al. [26], Triantafillou and Antonopuolos [11], and ACI 440 [23]; all of them can be utilized in SA2 program. However, the results presented in this study are based on the model of Chen and Teng [25] for the control of the debonding strain of the FRP sheets.

4. Verification of analytical procedures

The analytical procedures in the current study are capable of determining the internal stresses and strains at any point in the cross section of the strengthened beams throughout the entire range of loading up to failure. To verify the procedure, the results of 15 experimental studies available in the literature are selected and analyzed by SA2 program. General characteristics of the selected beams are given in Table 1; more details on each beam can be found in the original references.

In Table 1, the strengthening scheme for each beam is characterized with 2 letters. The first letter is S, U, or W with S representing the side bonding, U standing for U-shape bonding, and W representing the full wrapping of FRP around the beam section. The second letter is C or S; C indicates that the FRP sheets are continuous along the shear span and S shows that strips of FRP sheets are intermittently used along the shear span. For example, U-C strengthening scheme presents the shear strengthening with continuous U-shape FRP sheets.

The beams shown in Table 1 were analyzed using SA2 program. The strains in the FRP sheets or steel reinforcing bars corresponding to shear forces in the section were obtained for the entire loading history. A comparison between the experimental and analytical results is given in Figure 8. As can be seen, there is good agreement between the analytical and experimental curves throughout the entire load history in most cases. However, in specimens B80-1, PU3, and PU4 (cases no. 11, 13, and 14 in Table 1), despite good agreement between the experimental and analytical curves of shear force versus strain in longitudinal reinforcement, the calculated maximum strain in longitudinal reinforcement of the beam is much larger than that in the measured one. In other words, an abrupt increase in the strain of reinforcing bars is observed in the analytical results due to yielding of steel in the aforementioned specimens, while the reinforcing bars in the actual tests did not yield. More scrutiny of

Table 1. Details of the design of the selected beams.

	Ref.	Specimen	b_w (mm)	Strengthening schemens	Fibers orientation	Fiber*
1	Adhikary et al. [27]	C-1	300	U-C	90°	C
2	Adhikary et al. [27]	C-4	300	W-C	90°	C
3	Adhikary et al. [27]	A-1	300	U-C	90°	A
4	Adhikary et al. [27]	A-4	300	W-C	90°	A
5	Adhikary and Mutsuyoshi [28]	B-4	150	S-C	90°	C
6	Adhikary and Mutsuyoshi [28]	B-5	150	S-C	0°/90°	C
7	Adhikary and Mutsuyoshi [28]	B-6	150	S-C	0°/90°	C
8	Adhikary and Mutsuyoshi [28]	B-8	150	U-C	90°	C
9	Khalifa and Nanni [29]	SO3-4	150	U-C	90°	C
10	Khalifa and Nanni [29]	SW3-2	150	U-C	0°/90°	C
11	Li et al. [32]	B80-1	130	U-C	45°/135°	C
12	Li et al. [32]	B80-2	130	U-C	45°/135°	C
13	Diagana et al. [33]	PU3	130	U-S	45°	C
14	Diagana et al. [33]	PU4	130	U-S	45°	C
15	Diagana et al. [33]	PC4	130	W-S	45°	C

* C: Carbon; A: Aramid.

the experimental results of these specimens indicates that although the maximum strain of the longitudinal bars has passed the reported yield strain of the steel ($\varepsilon_y = 0.0026$), the actual test results do not indicate yielding of the bars. To justify this behavior, it can be stated that probably the actual yield strain of the reinforcing bars used in the tests is somewhat higher than the reported yield strain. Therefore, the lack of agreement between the analytical and experimental curves in Figure 8 for specimens B_{80-1}, PU_3, and PU_4 in the last steps of the loading history can be attributed to the assumption of a lower yield strain for the reinforcing bar than for actual tests. Overall, it can be concluded that the analytical procedures presented here based on MCFT and SA2 program are capable of predicting the behavior of the RC beams strengthened with FRP sheets for shear throughout the entire loading history.

The theoretical procedures discussed above as well as the SA2 program are capable of predicting the ultimate shear capacity of the RC beams strengthened with FRP sheets. To evaluate the accuracy of the method for such prediction, 69 RC beams were selected from the published test results. The beams were strengthened with FRP sheets and loaded up to failure. The details of these beams and the FRP sheet used for strengthening are presented in Table 2. It is observed from the table that the selected beams cover a rather full range of the effective parameters on the behavior of the beam, including the cross section of the beam, the strengthened configuration, the inclination of the FRP sheets, and the shear span-to-depth ratio a/d. The parameter V_{ex} in Table 2 is the reported shear capacity of the strengthened beam. Although only the shear forces in the shear span at the failure of the beam have been reported as shear capacity in the original studies, in the analysis presented here, the capacity is the outcome of the combined effects of shear force and bending moment at critical sections.

The ultimate capacity of the RC beams determined based on the analytical methods strongly depends on the limit state conditions. The limiting state conditions are determined based on different expected modes of failure. Here, three possible modes of failure are shear failure, flexural failure, and debonding of FRP layers from the concrete surface. The shear failure occurs when the equilibrium and compatibility equations as well as the stress-strain relationship presented for the RC element strengthened with FRP sheets are not satisfied at least in one of the layers of the beam. Such conditions are provided when the tensile strains in the concrete increase considerably. On the other hand, the flexural failure happens when the extreme compressive strain of concrete reaches its ultimate strain at failure, ε_{cu}. In the current analysis, the ultimate strain of concrete is taken as $\varepsilon_{cu} = 0.0035$, as a rather realistic value for most practical cases.

The debonding mode of failure occurs when the strain in the fibers reaches a limiting strain correspond-

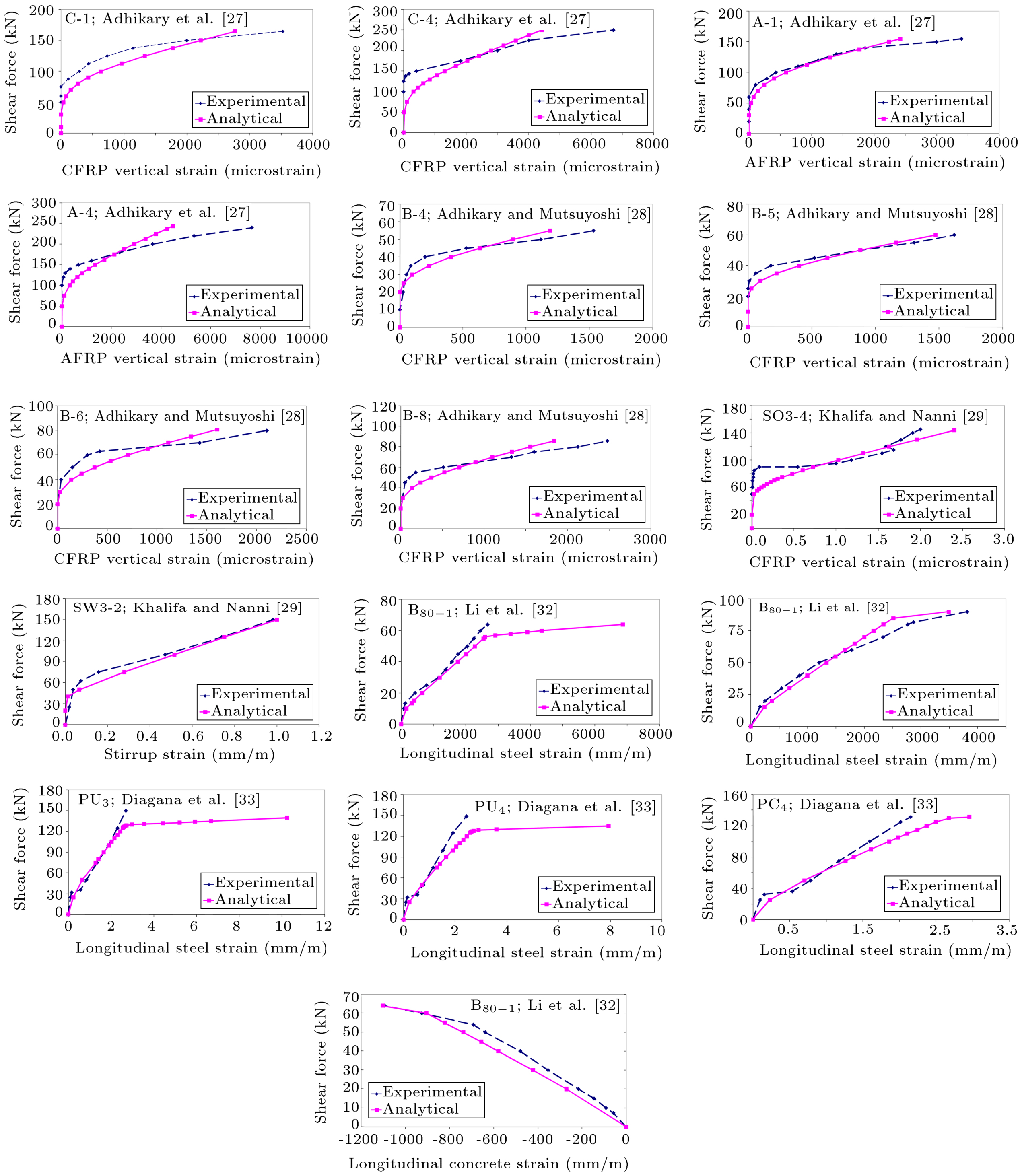

Figure 8. Comparison between analytical and experimental results for beams.

ing to debonding of the sheet from concrete. Many recommendations are found on the limiting strain of debonding of FRP sheets in the literature; some of the related references including ACI 440 [23] were referred to in the previous section. Here, the effect of debonding is first excluded and then included in the analysis, as described in the following:

1. The analyses are first performed neglecting the debonding mode of failure and including both shear and flexure modes of failure. This assumption is justified by noticing that some reports indicate combined shear and debonding failures, and/or combined flexure and debonding failures [27-31].

The predicted shear capacities of the selected

Table 2. Comparicon between analytical and experimental ultimate shear capacities.

No.	Ref.	Specimen	Sec.*	b_w (mm)	d (mm)	a/d	Strength schemes	Fiber**	Fibers orient.	ε_u	V_{ex} (kN)	Without debonding		With debonding	
												V_{pr} (kN)	V_{ex}/V_{pr}	V_{pr} (kN)	V_{ex}/V_{pr}
1	Al-Sulaimani [34]	SO	R	150	125	3.2	S-S	G	90°	0.0049	41.5	39.4	1.05	38.3	1.07
2	Al-Sulaimani [34]	SP	R	150	125	3.2	S-S	G	90°	0.0049	41.2	49.5	0.83	44.9	0.92
3	Al-Sulaimani [34]	WO	R	150	125	3.2	S-C	G	90°	0.0029	42.0	39.0	1.08	38.3	1.1
4	Al-Sulaimani [34]	WP	R	150	125	3.2	S-C	G	90°	0.0029	45.2	48.8	0.93	43.0	1.05
5	Al-Sulaimani [34]	JO	R	150	125	3.2	U-C	G	90°	0.0033	50.1	40.0	1.25	39.8	1.26
6	Al-Sulaimani [34]	JP	R	150	125	3.2	U-C	G	90°	0.0033	62.3	50.1	1.24	47.9	1.3
7	Chajes et al. [35]	A1	T	63.5	152.5	2.7	U-C	A	0°/90°	0.0073	38.7	30.4	1.27	25.8	1.5
8	Chajes et al. [35]	A2	T	63.5	152.5	2.7	U-C	A	0°/90°	0.0073	30.0	30.4	0.99	25.8	1.16
9	Chajes et al. [35]	E1	T	63.5	152.5	2.7	U-C	G	0°/90°	0.0097	36.7	27.0	1.36	23.9	1.54
10	Chajes et al. [35]	E2	T	63.5	152.5	2.7	U-C	G	0°/90°	0.0097	34.0	27.0	1.26	23.9	1.42
11	Chajes et al. [35]	G1	T	63.5	152.5	2.7	U-C	Gr	0°/90°	0.0071	35.5	30.8	1.15	26.2	1.36
12	Chajes et al. [35]	G2	T	63.5	152.5	3.7	U-C	Gr	0°/90°	0.0071	36.4	30.8	1.18	26.2	1.39
13	Norris et al. [36]	IE	R	127	153	3	U-C	C	90°	0.004	70.0	54.6	1.28	54.1	1.29
14	Norris et al. [36]	ID	R	127	153	3.7	U-C	C	45°/135°	0.004	32.5	29.2	1.11	22.7	1.43
15	Khalifa and Nanni [30]	BT2	T	150	355	3	U-C	C	90°	0.0038	155.0	162.5	0.95	141.7	1.09
16	Khalifa and Nanni [30]	BT3	T	150	355	3	U-C	C	0°/90°	0.0038	157.5	181.6	0.87	142.9	1.1
17	Khalifa and Nanni [30]	BT4	T	150	355	3	U-S	C	90°	0.0057	162.0	151.7	1.07	120.5	1.34
18	Khalifa and Nanni [30]	BT5	T	150	355	3	U-S	C	90°	0.0057	121.5	151.7	0.8	120.5	1.01
19	Li et al. [37]	B_{01}	R	130	270	3	U-C	C	45°/135°	0.005	65.0	70.0	0.93	40.1	1.62
20	Li et al. [37]	B_{02}	R	130	270	3	U-C	C	45°/135°	0.005	88.0	73.4	1.2	53.0	1.66
21	Li et al. [37]	B_{03}	R	130	270	3	U-C	C	45°/135°	0.005	85.0	75.0	1.13	60.2	1.41
22	Li et al. [37]	B_{11}	R	130	270	3	U-C	C	45°/135°	0.005	64.0	71.0	0.9	60.5	1.06
23	Li et al. [37]	B_{21}	R	130	270	3	U-C	C	45°/135°	0.005	76.0	74.4	1.02	60.5	1.26

*T: T-Shape, R: Rectangular; ** C: Carbon, G: Glass, A: Aramid

Table 2. Comparicon between analytical and experimental ultimate shear capacities (continued).

No	Ref.	Specimen	Sec.*	b_w (mm)	d (mm)	a/d	Strength schemes	Fiber**	Fibers orient.	ε_u	V_{ex} (kN)	Without debonding		With debonding	
												V_{pr} (kN)	V_{ex}/V_{pr}	V_{pr} (kN)	V_{ex}/V_{pr}
24	Li et al. [37]	B_{22}	R	130	270	3	U-C	C	45°/135°	0.005	88.0	75.0	1.17	60.8	1.45
25	Li et al. [37]	B_{23}	R	130	270	3	U-C	C	45°/135°	0.005	87.0	74.7	1.16	60.8	1.43
26	Li et al. [37]	B_{31}	R	130	270	3	U-C	C	45°/135°	0.005	88.0	74.4	1.18	60.8	1.45
27	Li et al. [37]	$B_{20\text{-}02}$	R	130	270	3	U-C	C	45°/135°	0.005	90.0	99.7	0.9	61.8	1.45
28	Khalifa and Nanni [30]	SO3-2	R	150	255	3	U-S	C	90°	0.0054	131.0	150.0	0.87	108.8	1.2
29	Khalifa and Nanni [30]	SO3-3	R	150	255	3	U-S	C	90°	0.0057	133.5	164.5	0.81	117.9	1.13
30	Khalifa and Nanni [30]	SO4-2	R	150	255	4	U-S	C	90°	0.0054	127.5	135.6	0.94	101.2	1.26
31	Khalifa and Nanni [30]	SO3-4	R	150	255	3	U-C	C	90°	0.0036	144.5	178.6	0.81	124.0	1.17
32	Khalifa and Nanni [30]	SO4-3	R	150	255	4	U-C	C	90°	0.0036	155.0	143.5	1.08	115.0	1.35
33	Khalifa and Nanni [30]	SW3-2	R	150	255	3	U-C	C	0°/90°	0.0033	177.0	150.0	1.18	109.9	1.61
34	Khalifa and Nanni [30]	SW4-2	R	150	255	4	U-C	C	0°/90°	0.0033	180.5	143.9	1.25	102.3	1.76
35	Khalifa and Nanni [30]	SO3-5	R	150	255	3	U-C	C	0°/90°	0.0036	169.5	181.8	0.93	124.7	1.36
36	Chaallal et al. [31]	G24-1L	T	122	343	2	U-C	C	90°	0.0098	258.0	209.4	1.23	207.1	1.25
37	Chaallal et al. [31]	G24-2L	T	122	343	2	U-C	C	90°	0.0008	253.5	212.6	1.19	212.6	1.19
38	Chaallal et al. [31]	G24-3L	T	122	343	2	U-C	C	90°	0.0006	258.0	214.2	1.2	214.2	1.2
39	Taljsten [38]	RC1	R	180	450	2.8	U-C	C	45°	0.0054	306.0	338.3	0.9	214.3	1.43
40	Taljsten [38]	C1	R	180	450	2.8	U-C	C	45°	0.0068	246.7	327.3	0.75	219.7	1.12
41	Taljsten [38]	C2	R	180	450	2.8	U-C	C	45°	0.0055	257.2	340.6	0.76	219.7	1.17
42	Taljsten [38]	C3	R	180	450	2.8	U-C	C	90°	0.0052	260.6	317.0	0.82	275.5	0.95
43	Wong and Vecchio [39]	RWOA-1	R	305	465	3.9	S-S	C	90°	0.0029	246.5	218.6	1.13	218.6	1.13
44	Wong and Vecchio [39]	RWOA-2	R	305	465	4.9	S-S	C	90°	0.003	228.5	220.3	1.04	220.3	1.04
45	Wong and Vecchio [39]	RWOA-3	R	305	465	6.9	S-S	C	90°	0.0034	218.0	208.4	1.05	208.4	1.05
46	Deniaud and Cheng [40]	T4S2-C45	T	140	350	3.1	U-C	C	45°	0.0044	219.0	191.3	1.15	135.7	1.61

*T: T-Shape, R: Rectangular; ** C: Carbon, G: Glass, A: Aramid

Table 2. Comparicon between analytical and experimental ultimate shear capacities (continued).

No.	Ref.	Specimen	Sec.*	b_w (mm)	d (mm)	a/d	Strength schemes	Fiber**	Fibers orient.	ε_u	V_{ex} (kN)	Without debonding		With debonding	
												V_{pr} (kN)	V_{ex}/V_{pr}	V_{pr} (kN)	V_{ex}/V_{pr}
47	Deniaud and Cheng [40]	T4S4-G90	T	140	350	3.1	U-C	G	90°	0.004	205.6	172.2	1.19	171.4	1.2
48	Deniaud and Cheng [40]	T4NS-G90	T	140	350	3.1	U-C	G	90°	0.004	159.0	147.4	1.08	108.8	1.46
49	Deniaud and Cheng [40]	T4S2-G90	T	140	350	3.1	U-C	G	90°	0.004	225.6	175.4	1.29	173.8	1.3
50	Diagana et al. [33]	PU_1	R	130	425	2.1	U-S	C	90°	0.0061	142.5	140.4	1.02	125.3	1.14
51	Diagana et al. [33]	PU_2	R	130	425	2.1	U-S	C	90°	0.0063	130.0	139.4	0.93	120.7	1.08
52	Diagana et al. [33]	PU_3	R	130	425	2.1	U-S	C	45°	0.0064	154.5	142.9	1.08	95.1	1.62
53	Diagana et al. [33]	PU_4	R	130	425	2.1	U-S	C	45°	0.0065	150.0	137.9	1.09	94.1	1.59
54	Diagana et al. [33]	PC_1	R	130	425	2.1	W-S	C	90°	---	177.5	141.9	1.25	---	---
55	Diagana et al. [33]	PC_2	R	130	425	2.1	W-S	C	90°	---	155.0	140.9	1.1	---	---
56	Diagana et al. [33]	PC_3	R	130	425	2.1	W-S	C	45°	---	145.5	145.2	1	---	---
57	Diagana et al. [33]	PC_4	R	130	425	2.1	W-S	C	45°	---	132.0	141.9	0.93	---	---
58	Lanniruberto and Limbimbo [41]	ST1A	R	150	318	2.8	W-C	G	90°	---	242.0	196.4	1.23	---	---
59	Adhikary and Mutsuyoshi [28]	B-4	R	150	170	3	S-C	C	90°	0.0036	58.6	73.3	0.8	62.8	0.93
60	Adhikary and Mutsuyoshi [28]	B-5	R	150	170	3	S-C	C	0°/90°	0.0036	60.3	77.2	0.78	63.0	0.96
61	Adhikary and Mutsuyoshi [28]	B-6	R	150	170	3	S-C	C	0°/90°	0.0037	80.8	80.9	1	76.5	1.06
62	Adhikary and Mutsuyoshi [28]	B-7	R	150	170	3	U-C	C	90°	0.0037	68.5	74.1	0.92	65.3	1.05
63	Adhikary [28]	B-8	R	150	170	3	U-C	C	90°	0.0038	85.8	77.2	1.11	75.2	1.14
64	Adhikary et al. [27]	C-1	R	300	245	4.1	U-C	C	90°	0.0038	165.0	224.2	0.74	165.4	1
65	Adhikary et al. [27]	C-4	R	300	245	4.1	W-C	C	90°	---	250.0	234.0	1.07	---	---
66	Adhikary et al. [27]	A-1	R	300	245	4.1	U-C	A	90°	0.0041	155.0	225.4	0.69	168.5	0.92
67	Adhikary et al. [27]	A-4	R	300	245	4.1	W-C	A	90°	---	244.0	234.7	1.04	---	---
68	Bousselham and Chaallal [42]	SBS01L	T	95	175	3	U-C	C	0°/90°	0.0055	59.3	58.1	1.02	47.9	1.24
69	Bousselham and Chaallal [42]	SBS02L	T	95	175	3	U-C	C	0°/90°	0.0039	68.5	65.8	1.04	51.7	1.33

*T: T-Shape, R: Rectangular; ** C: Carbon, G: Glass, A: Aramid

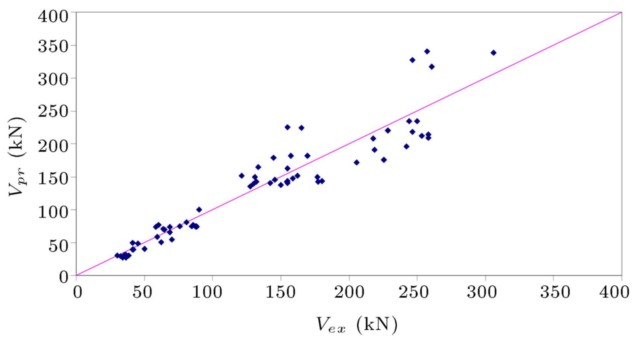

Figure 9. Comparison between analytical and experimental results without effect of debonding.

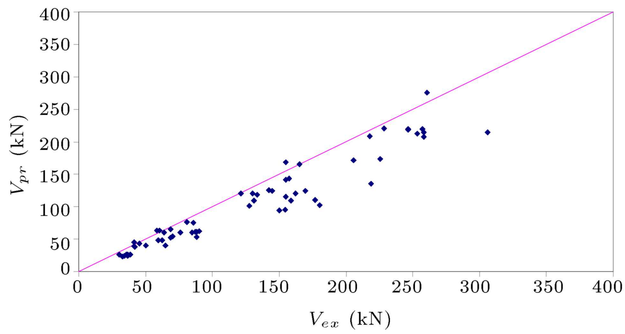

Figure 10. Comparison between analytical and experimental results with effect of debonding.

beams computed by SA2 program are shown in Table 2 with V_{pr} in the column titled "without debonding" and the ratios of experimental to predicted shear capacities, V_{ex}/V_{pr}, in the next column of the table. The mean value is 1.04 and the corresponding standard deviation is 0.026.

Furthermore, a comparison between the predicted and experimentally observed shear capacities is presented in Figure 9. The accuracy of the analytical procedure presented in this paper for the shear analysis of RC beams strengthened with FRP sheets can be demonstrated by the results of Table 2 and/or Figure 9.

It is observed from Figure 9 that the beams under investigation can be categorized in two groups:

(a) The specimens for which the estimated shear capacities are higher than their measured capacities (points above inclined line in Figure 9);

(b) The specimens for which the calculated shear capacities are in the safe margin and lower than their experimentally measured capacities (points below inclined line in Figure 9).

However, it can be noted that in the specimens of group (a), debonding of FRP sheets from concrete has been reported as an integral mode of failure in most cases. For such cases, it is evident that since the analytical results in Figure 9 are only based on inclusion of shear and flexural modes of failure without considering the effect of debonding of FRP composites, the predicted results are larger than the observed shear capacities. This means that the inclusion of the debonding mode of failure in SA2 program leads to more reliable predictions of shear capacities of strengthened RC beams with FRP sheets, as can be seen in the following.

2. The analyses are also performed with the inclusion of all possible modes of failure. To include the effect of debonding, a limiting state of strain for debonding of the FRP has to be defined. Here, the strain of the fibers corresponding to their debonding is arbitrarily computed with the expressions suggested by Chen and Teng [25]. The selection is partly because the model of Chen and Teng includes more parameters affecting the debonding limiting strain than other available models do. The calculated strains in the fibers corresponding to the debonding of FRP composites for the selected beams are shown in Table 2 with variable ε_u. Furthermore, the predicted shear capacities of the selected beams computed by SA2 program with the inclusion of the effect of debonding of FRP sheets are shown in Table 2 with the variable V_{pr} in the column titled "with debonding." Also, the ratios of the experimentally observed to predicted shear capacities, V_{ex}/V_{pr}, are presented in the last column of the table; the mean value and the corresponding standard deviation are 1.26 and 0.043, respectively. Figure 10 provides a comparison between the observed and predicted results when debonding of FRP sheets is included as a failure mode in the analysis. The results presented in Table 2, or in Figure 10, show that if debonding mode of failure is included in the analytical procedures for shear analysis of concrete beams strengthened with FRP sheets, the method is capable of good and safe prediction of the ultimate shear capacity of the beam. However, the accuracy of the results in this case depends on the suitability and capability of the model for debonding failure of the FRP sheets.

5. A case study of the effect of debonding of FRP sheets on shear capacity of strengthened RC beams

Debonding of FRP sheets from the surface is an important phenomenon affecting the expected flexural and shear capacities of the RC beams strengthened with FRP composites. In fact, debonding of FRP sheets from concrete surface prevents full development of the tensile strength of the fibers. Here, the effect of

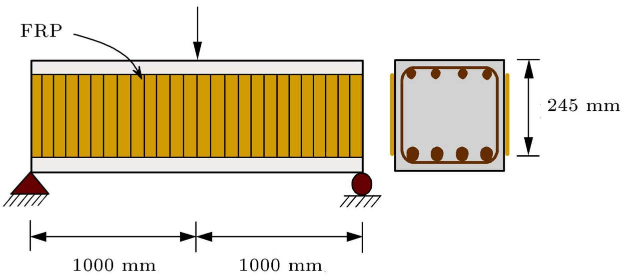

Figure 11. Geometrical and mechanical properties of beams B1 and B2: $h = b_w = 300$ mm; $E_s = 200$ GPa; $E_f = 230$ GPa. Top longitudinal reinforcement = $4\phi22$; and bottom longitudinal reinforcement = $4\phi32$. FRP ratio = 0.0011; $f'_c = 28$ MPa; and $f_y = 300$ MPa. Steel shear reinforcement: B1: 0.00063 ($\phi6$@300 mm), and B2: 0.0025 ($\phi6$@75 mm).

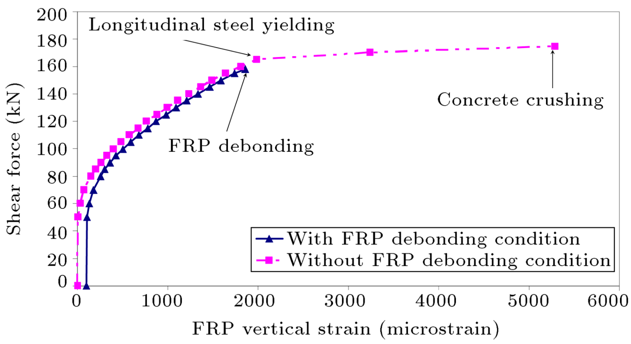

Figure 12. Shear force versus FRP strain history for beam B1.

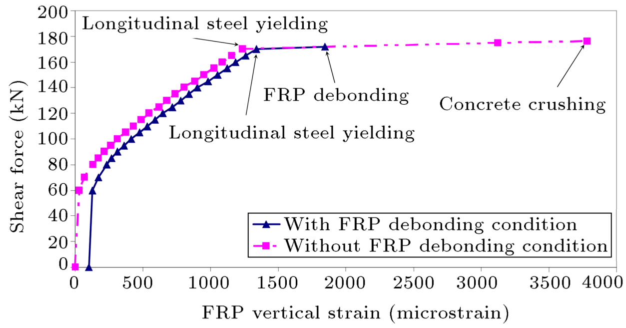

Figure 13. Shear force versus FRP strain history for beam B2.

debonding of FRP sheets on the ultimate shear capacity as well as the ductile behavior of the strengthened RC beams is studied using the procedures of analysis discussed before and the SA2 program.

RC beams B1 and B2 are defined with their dimensional and mechanical characteristics given in Figure 11. It is seen in Figure 11 that the only difference between beam B1 and beam B2 is the transverse reinforcement ratio, where the interval of shear stirrups in beam B2 is four times tighter than that of beam B1. The limiting strain of fibers corresponding to debonding of FRP sheets from concrete surface of both beams B1 and B2 is computed as $\varepsilon_u = 0.00357$, using the model suggested by Chen and Teng [25]. The beams are analyzed by the SA2 program, with and without debonding of FRP sheets. The analysis without the inclusion of debonding mode of failure is interpreted as the real behavior of the beams when debonding is prevented by means of mechanical anchorages of the FRP sheets or nailing the sheets into the concrete. The variations of the shear forces in beams B1 and B2 versus the maximum vertical strain in FRP for the entire loading history are shown in Figures 12 and 13, respectively. Each figure shows the results of the analysis with and without inclusion of debonding mode of failure; however, the analytical curves with the effect of debonding included are horizontally shifted 100 units to the right for clarity.

It is observed in Figure 12 that the shear failure of beam B1 is sudden and brittle due to debonding of FRP sheets. However, when debonding of FRP sheets from the surface of the sides of the beam is prevented, both higher shear capacity and ductile behavior before failure of the beam are observed. On the other hand, Figure 13 indicates that beam B2 has the same shear capacity and is ductile before impending shear failure, no matter if debonding of FRP sheets is prevented or permitted. In other words, special provisions to prevent occurrence of debonding of FRP sheets in beam B2 are effective neither in increasing the ultimate shear capacity nor in the mode of failure, although they increase the shear ductility of the strengthened RC beam to some extent.

The results of analyses of the strengthened beams B1 and B2 show that preventing debonding of FRP sheets neither increases the shear capacity nor changes the failure mechanism in all cases. In fact, if a strengthened beam fails due to debonding of the sheets, while the longitudinal reinforcement has yielded, preventing debonding of the sheets by mechanical anchorages or any other means does not improve the ultimate shear capacity of the beam. On the other hand, in the case of brittle failure mechanism, i.e., the failure of the strengthened RC beam due to debonding of the FRP sheets while the longitudinal reinforcing bars have not yielded, special provisions to prevent debonding of FRP sheets simultaneously increase the ultimate shear capacity and change the failure mechanism from brittle to ductile behavior. Preventing debonding in this case can be considered economical and useful for higher shear capacities and for achieving a ductile failure.

Different variables affect the yielding of the longitudinal reinforcement prior to shear failure, e.g., the transverse reinforcement ratio, the a/d ratio, the longitudinal reinforcement ratio, the ratio of FRP, and the mechanical properties of the materials used. The analytical procedures presented in this paper as well as the SA2 program provide an effective tool to determine the ranges of the variables in which preventing of debonding of FRP sheets for shear strengthening is economically justifiable and structurally suitable.

6. Results and discussions

In this study, the modified compression field theory was used for the analysis of RC beams externally strengthened for shear with FRP sheets. The equilibrium and compatibility equations and the stress-strain relationships of constituent materials were extended to a membrane element of RC strengthened with FRP sheets. Then, the relations were developed for the whole beam by dividing the beam section into separate layers. A computer program was developed based on this procedure. Comprehensive analyses were performed first on test results available in the literature for 15 RC beams and then on additional 69 RC beams. All beams had been strengthened for shear capacity with FRP sheets and monolithically loaded up to failure. Comparison between the experimentally observed and analytically predicted results showed close agreement within the entire range of loading up to the failure of the beams. It was also shown that the effect of debonding of the FRP sheets from concrete surfaces could be easily included in the analytical procedures using an appropriate model for estimation of the limiting strain of the fibers corresponding to the debonding of the sheets.

A complementary case study performed on a sample beam showed that inclusion of debonding of the FRP sheet in the analysis of the strengthened RC beams neither increased the shear capacity nor affected the failure mechanism in some cases. An important conclusion of this study is that preventing debonding of the FRP sheets from side faces of the beam by means of mechanical anchorage is rational and useful only if longitudinal tensile reinforcements yield prior to debonding of the sheets. Such conditions can be verified by performing the analysis for the particular combination of the longitudinal and transverse reinforcement, the a/d ratio, and using the mechanical properties of the materials.

Nomenclature

θ_1	Orientation of the fibers of FRP sheets
f_x	Applied normal stresses in x direction
ε_x	Strains in RC element in x direction
v_{xy}	Applied shear stress to the RC element
ε_{cx}	Strain in the concrete in x direction
ε_{sx}	Strain of longitudinal steel bars
ε_{fx}	Strain of fibers of the FRP in x direction
ε_1	Tensile principal strain in concrete element
θ	Angle of plane of principal strain
f_{f1}	Stress in fibers in θ_1 direction
A_c	Net section area of concrete
ρ_{sx}	Ratio of the longitudinal reinforcing bars
ρ_{f1}	Ratio of fibers in θ_1 direction
A_{sx}	Section area of longitudinal reinforcing bars
θ_c	Inclination angle of principal plane of stress
f_{c2}	Compressive principal stresses in the concrete
ε_s	Strain of the reinforcing bars
f'_c	Compressive strength of the concrete cylinder
ε'_c	Compressive strain of concrete
f_{cr}	Stress corresponding to cracking of concrete in tension
f_f	Stress in the FRP
t_f	Thickness of FRP sheets
w_f	Width of the FRP sheets
s_f	Spacing of FRP sheets
θ_2	Orientation of fibers of the FRP sheets
f_y	Applied normal stresses in y direction
ε_y	Strains in RC element in y direction
γ_{xy}	Shear strain in the RC element
ε_{cy}	Strain in the concrete in y direction
ε_{sy}	Strain of transverse steel bars
ε_{fy}	Strain of fibers of the FRP in y direction
ε_2	Compressive principal strain in concrete element
v_{cxy}	Shear stress in concrete
f_{f2}	Stress in fibers in θ_2 direction
d	Element dimension
A	Cross section area
ρ_{f2}	Ratio of fibers in θ_2 direction
b	Thickness of the element
t_{f1}	Thickness of FRP in θ_1 direction
A_{sy}	Section area of transverse reinforcing bars
f_{c1}	Tensile principal stresses in the concrete
E_s	Modulus of elasticity of steel
f_y	Yield strength of the reinforcing bars
$f_{c2\max}$	Compressive strength of concrete while the tensile stresses are present in the perpendicular direction
ε_{cr}	Strain corresponding to cracking of concrete in tension

ε_f Strain in the FRP

b_w Web width of the beam

References

1. Denton, S.R., Shave, J.D., and Porter, A.D. "Shear strengthening of reinforced concrete structures using FRP composites", *Proc. of the Second Int. Conf. on Advanced Polymer Composites for Structural Applications in Construction*, Guildford, University of Surry, UK, pp. 134-143 (2004).
2. Chen, J.F. and Teng, J.G. "Shear capacity of fiber-reinforced polymer-strengthened reinforced concrete beams: fiber reinforced polymer rupture", *J. of Struct. Eng.*, **129**(5), pp. 615-625 (2003).
3. Chen, J.F. and Teng, J.G. "Shear capacity of FRP-strengthened RC beams: FRP debonding", *Const. Build. Mat.*, **17**(1), pp. 27-41 (2003).
4. Colotti, V., Spadea, G., and Swamy, R.N. "Analytical model to evaluate failure of plated reinforced concrete beams strengthened for shear", *ACI Struct. J.*, **101**(6), pp. 755-764 (2004).
5. Colotti, V. and Swamy, R.N. "Unified Analytical approach for determining shear capacity of RC beams strengthened with FRP", *Eng. Struct.*, **33**(3), pp. 827-842 (2011).
6. Kim, G.Y., Sim, J.O., and Oh, H.O. "Shear strengthened RC beams with FRPs in shear", *Const. Build. Mat.*, **22**(6), pp. 1261-1270 (2008).
7. Lu, X.Z., Chen, J.F., Ye, L.P., Teng, J.G., and Rotter, J.M. "RC beams shear-strengthened with FRP: Stress distribution in the FRP reinforcement", *Const. Build. Mat.*, **23**(4), pp. 1544-1554 (2009).
8. Perera, R., Barchin, M., Arteaga, A., and Diego, A. "Prediction of the ultimate strength of reinforced concrete beams FRP-strengthened in shear using neural networks", *Composites: Part B*, **41**(4), pp. 287-298 (2010).
9. Tanarslan, H.M. "Predicting the capacity of RC beams strengthened in shear with side-bonded FRP reinforcements using artificial neural networks", *Compos. Interf.*, **18**(7), pp. 587-614 (2011).
10. Triantafillou, T.C. "Shear strengthening of reinforced concrete beams using epoxy-bonded FRP composites", *ACI Struct. J.*, **95**(2), pp. 107-115 (1998).
11. Triantafillou, T.C. and Antonopuolos, C.P. "Design of concrete flexural members strengthened in shear with FRP", *J. Compos. Constr.*, **4**(4), pp. 198-205 (2000).
12. Teo, W. and Hor, Y. "Suitability of optimized truss model to predict the FRP contribution to shear resistance for externally bonded FRP strengthened RC beams without internal stirrups", *Composites Part B: Engineering*, **80**, pp. 385-398 (2015).
13. Sayed, A.M., Wang, X., and Wu, Z. "Finite element modeling of the shear capacity of RC beams strengthened with FRP sheets by considering different failure modes", *Const. Build. Mat.*, **59**, pp. 169-179 (2014).
14. Colotti, V. "Shear interaction effect between transverse reinforcements in FRP-strengthened RC beams", *Composites Part B: Engineering*, **45**(1), pp. 1222-1233 (2013).
15. Domenico, D. "RC members strengthened with externally bonded FRP plates: A FE-based limit analysis approach", *Composites Part B: Engineering,* **71**, pp. 159-174 (2015).
16. Oller, E., Marí, A., Bairán, J.M., and Cladera, A. "Shear design of reinforced concrete beams with FRP longitudinal and transverse reinforcement", *Composites Part B: Engineering*, **74**(1), pp. 104-122 (2015).
17. Colotti, V. "Mechanical shear strength model for reinforced concrete beams strengthened with FRP materials", *Construction and Building Materials*, **124**, pp. 855-865 (2016).
18. Lee, D.H., Han, S.J., Kim, K.S., and Lafave, J.M. "Shear strength of reinforced concrete beams strengthened in shear using externally-bonded FRP composites", *Composite Structures*, **173**, pp. 177-187 (2017).
19. Malek, A.M. and Saadatmanesh, H. "Ultimate shear capacity of reinforced concrete beams strengthened with web-bonded fiber-reinforced plastic plates", *ACI Struct. J.*, **95**(4), pp. 391-399 (1998).
20. Gendron, G., Picard, A., and Guerin, M.C. "A theoretical study on shear strengthening of reinforced concrete beams using composite plates", *Compos. Struct*, **45**(4), pp. 303-309 (1999).
21. Stratford, T. and Burgoyne, C. "Shear analysis of concrete with brittle reinforcement", *J. Compos. Constr.*, **7**(4), pp. 323-330 (2003).
22. Vecchio, F.J. and Collins, M.P. "The modified compression-field theory for reinforced concrete elements subjected to shear", *ACI Struct. J.,* **83**(2), pp. 219-231 (1986).
23. ACI Committee 440, *Guide for the Design and Construction of Externally Bonded FRP Systems for Strengthened Concrete Structures*, ACI 440.2R-08 (2008).
24. Vecchio, F.J. and Collins, M.P. "Predicting the response of reinforced concrete beams subjected to shear using modified compression field theory", *ACI Struct. J.*, **85**, pp. 258-268 (1998).
25. Chen, J.F. and Teng, J.G. "Anchorage strength models for FRP and sheet plates bonded to concrete", *J. of Struct. Eng.*, **127**(7), pp. 784-791 (2001).
26. Khalifa, A., Gold, W.J., Nanni, A., and Abdel Aziz, M.I. "Contribution of externally bonded FRP to shear capacity of RC flexural members", *J. Compos. Constr.*, **2**(4), pp. 195-202 (1998).
27. Adhikary, B.B., Mutsuyoshi, H., and Ashraf, M. "Shear strengthening of reinforced concrete beams using fiber-reinforced polymer sheets with bonded anchorage", *ACI Struct. J.*, **101**(5), pp. 660-668 (2004).
28. Adhikary, B.B. and Mutsuyoshi, H. "Behavior of concrete beams strengthened in shear with carbon-fiber sheets", *J. Compos. Constr.*, **8**(3), pp. 258-264 (2004).

29. Khalifa, A. and Nanni, A. "Rehabilitation of rectangular simply supported RC beams with shear deficiencies using CFRP composites", *Const. Build. Mat.*, **16**(3), pp. 135-146 (2002).

30. Khalifa, A. and Nanni, A. "Improving shear capacity of existing RC T-section beams using CFRP composites", *Cem. Conc. Compos.*, **22**(3), pp. 165-174 (2000).

31. Chaallal, O., Shahawy, M., and Hassan, M. "Performance of reinforced concrete T-girders strengthened in shear with carbon fiber-reinforced polymer fabric", *ACI Struct. J.*, **99**(3), pp. 335-343 (2002).

32. Li, A., Diagana, C., and Delmas, Y. "Shear strengthened effect by bonded composite fabrics on RC beams", *Composites: Part B*, **33**(3), pp. 225-239 (2002).

33. Diagana, C., Li, A., Gedalia, B., and Delmas, Y. "Shear strengthening effectiveness with CFF strips", *Eng. Struct.*, **25**(4), pp. 507-516 (2003).

34. Al-Sulaimani, G.J., Sharif, A., Basunbul, I.A., Baluch, M.H., and Ghaleb, B.N. "Shear repair for reinforced concrete by fiberglass plate bonding", *ACI Struct. J.*, **91**(3), pp. 458-464 (1994).

35. Chajes, M.J., Januszka, T.F., Mertz, D.R., Thomson, T.A., and Finch, W.W. "Shear strengthening of reinforced concrete beams using externally applied composites fabrics", *ACI Struct. J.*, **92**(3), pp. 295-303 (1995).

36. Norris, T., Saadatmanesh, H., and Ehsani, M.R. "Shear and flexural strengthening of R/C beams with carbon fiber sheets", *J. of Struct. Eng.*, **123**(7), pp. 903-911 (1997).

37. Li, A., Diagana, C., and Delmas, Y. "CFRP contribution to shear capacity of strengthened RC beams", *Eng. Struct.*, **23**(10), pp. 1212-1220 (2001).

38. Taljsten, B. "Strengthening concrete beams for shear with CFRP sheets", *Const. Build. Mat.*, **17**(1), pp. 15-26 (2003).

39. Wong, R.S.Y. and Vecchio, F.J. "Towards modeling of reinforced concrete members with externally bonded fiber-reinforced polymer composites", *ACI Struct. J.*, **100**(1), pp. 47-55 (2003).

40. Deniaud, C. and Cheng, J.J.R. "Reinforced concrete T-beams strengthened in shear with fiber reinforced polymer sheets", *J. Compos. Constr.*, **7**(4), pp. 302-310 (2003).

41. Lanniruberto, U. and Limbimbo, M. "Role of reinforced plastic sheets in shear response of reinforced concrete beams: experimental and analytical results", *J. Compos. Constr.*, **8**(5), pp. 415-424 (2004).

42. Bousselham, A. and Chaallal, O. "Effect of transverse steel and shear span on the performance of RC beams strengthened in shear with CFRP", *Composites: Part B*, **37**(1), pp. 37-46 (2006).

Biographies

Davood Mostofinejad is a Professor in the Department of Civil Engineering at Isfahan University of Technology (IUT), Isfahan, Iran; currently, he attends University of California, Irvine (UCI), as visiting professor. He received his BSc and MSc from Tehran University and Isfahan University of Technology in 1985 and 1987, respectively, and his PhD from Carleton University, Ottawa, Canada, in 1997. His research interests include application of FRP composites to concrete and masonry structures, repair and rehabilitation of damaged RC structures, concrete technology, and biological treatment of concrete.

Mohsen Noormohamadi is a Lecturer at Azad University of Saveh, Saveh, Iran. He received his BSc from Azad University of Najafabad in 2003 and his MSc from Isfahan University of Technology in 2006. He is currently a PhD candidate at Isfahan University of Technology.